stellarator news

Published by Fusion Energy Division, Oak Ridge National Laboratory
Building 5700 P.O. Box 2008 Oak Ridge, TN 37831-6169, USA

Editor: James A. Rome Issue 96 January 2005
E-Mail: jar@ornl.gov Phone (865) 482-5643
On the Web at *http://www.ornl.gov/sci/fed/stelnews*

Delivery of first non-planar coil and plasma vessel elements for W7-X

The first nonplanar superconducting coil of the modular stellarator Wendelstein 7-X (W7-X) has been delivered to Griefswald for assembly, arriving on site just before the end of 2004 (Fig.1). A total of 50 nonplanar coils — in a variety of 5 different coil types — provide the standard magnetic field configuration with low shear and an edge $\iota(a) = 1.0$ at minor radius $a = 52$ cm.

Fig. 1. The first superconducting coil AAB18 — approximately 3.5 m high and 2.5 m wide with a total weight of 5.5 tonnes — was shipped from the Babcock Noell Nuclear workshop at Zeitz to the Greifswald site and unloaded at the coil preparation hall on 30 December 2004. Copper stripes seen on the coil are part of the cooling system for the casing. Photo: W. König.

The nonplanar coils are among the most challenging components of the W7-X device, and a number of engineering problems had to be resolved during production:

- Each coil is separately fastened to the central support ring of W7-X to allow for motion during cooldown and under magnetic field variation. Forces between neighboring coils are taken by highly precise support elements, which recently had to be modified to withstand the extremely high mechanical loads. The new design was developed after prototype and welding tests in summer 2004. As a consequence, the routing of helium cooling pipes in these areas, which cool the casing via copper stripes welded to each coil, also had to be modified.
- The insulation of the cables for quench detection turned out to be insufficient for the expected high voltages during a rapid shutdown. All quench detection cables have subsequently been exchanged to withstand the specified 13 kV.

In this issue . . .

Fig. 2. Queuing for assembly: Like the kit for a three-dimensional stellarator puzzle, sectors of the W7-X plasma vessel are waiting for assembly. The plasma vessel contour follows the shape of the plasma. Two sectors form a stellarator symmetric half-module; a total of 20 sectors is required for the whole vessel. Altogether they are assembled from 200 wedged ring elements (see, e.g., the sector on the right-hand side). Cooling pipes are mounted on the outer side of the sectors on the left. Saddle coils have been installed as the first components of the magnetic diagnostics. Photo: MAN DWE GmbH.

- The cast stainless steel casings of the coils showed a number of unacceptable voids, which had to be removed. The voids were detected during a systematic scan of all casings with synchrotron radiation from a linear accelerator.

Meanwhile, seven coils (three planar and four nonplanar) have been tested at their design current (around 17 kA) at low temperature at the test rig at Commissariat à l'Energie Atomique (CEA) in Saclay, France. A Paschen test (pressure variation at fixed high voltage) was also performed to probe the robustness of the design to high-voltage (HV) breakdown that would occur during a combined vacuum leakage and quench event.

Assembly of plasma vessel elements, the superinsulation, and the thermal shield began in September at Greifswald (Fig. 2). Figure 3 shows a part of the vessel (lower left) with cooling pipes on its vacuum side followed by the multilayer insulation ("superinsulation") and the thermal shield to the right. The thermal shield is segmented into 200 panels that cover the whole plasma vessel. They consist of fiberglass-reinforced epoxy with an aluminum layer on the outboard side that faces the cold coils. The shield panels include a copper net for thermal conductivity, from which copper braids (see Fig. 3) conduct the heat flux to cooling pipes with helium flowing at about 40 K (not yet installed in the figure). The panels cover a superinsulation consisting of 20 layers of aluminized Kapton foils with interlayers of glass silk.

From the plasma vessel, a heat flux of <9 W/m² across the superinsulation is allowed to keep the shield at its design temperatures of 80–90 K. The specified power flux to coils is 1.5 W/m². Geometrical tolerances are small because of the narrow distances to the nonplanar superconducting coils, which will be located just outside the shield. The total height available for the shield is 25 mm — at some positions even less; for comparison, the tolerances of the plasma vessel itself are ±2 mm. All components, plasma vessel, thermal shield, and the superinsulation are supplied by MAN DWE, Germany.

Matthias Hirsch for the W7-X Team
Max-Planck-Institut für Plasmaphysik
Teilinstitut Greifswald
Wendelsteinstraße 1
D-17491 Greifswald
Germany

E-mail: matthias.hirsch@ipp.mpg.de

Phone: +49-3834-88-2536
FAX: +49-3834-88-2009

Fig. 3. Detail of plasma vessel (lower left) surrounded by the multilayer insulation ("superinsulation") with the thermal shield to the right. The superinsulation hidden below the shield is visible only at its edge. Photo: Beate Kemnitz.

Transient electron heat transport in LHD plasmas with and without an electron internal transport barrier

Introduction

Electron heat transport is now one of the most important issues in confinement studies because the fusion power in a reactor is directly absorbed by electrons from the high-energy alpha particles. The many experimental results indicate that the radial electron heat transport is anomalously higher than neoclassical theory, and thus heat transport is considered to be driven by turbulent processes.

Some local transport models based on temperature-gradient-driven turbulence indicate that the heat transport is nonlinear, and thus the electron heat diffusivity χ_e has a dependence on electron temperature T_e and/or its gradient ∇T_e [1, 2]. Nonlinear models based on the "critical gradient scale length" can explain some of the tokamak-type stiffness [3]. On the other hand, the transport phenomenon known as "profile stiffness" is weak or absent in helical systems. In fact, although the global confinement scaling is similar to ELMy H-mode scaling [4], no evidence for the tokamak-like stiffness is observed in LHD. (Recently, a different type of stiffness has been observed in high density plasmas in the Large Helical Device (LHD) [5].) Therefore, the validity of nonlinear transport models based on turbulence should be tested in helical systems to establish first-principle transport models. To study the nonlinearity of heat transport and to clarify the role of turbulence on the electron heat transport, transient transport analysis is recognized as a very powerful tool because it can yield $\partial q_e/\partial T_e$ and $\partial q_e/\partial \nabla T_e$, where q_e is the electron heat flux [6].

Recent experimental progress on LHD enables us to make a more extensive comparison of the transient response in plasmas not only without an internal transport barrier (ITB), but also with an ITB. In helical systems, the electron ITB is observed to be associated with the transition from the ion root to the electron root (involving strong $\boldsymbol{E} \times \boldsymbol{B}$ shear induced by neoclassical bifurcation of the radial electric field) [7–9]. The transport barriers are considered to be formed by suppression of turbulence-induced transport in both helical systems and tokamaks; however, some important questions, such as whether the transport in the ITB is diffusive or convective, and whether it remains stiff, have not yet been answered. Transient experiments are also relevant to clarify these issues.

Cold pulse experiments in plasma without ITB

In order to induce a cold pulse, a tracer encapsulated solid pellet (TESPEL [10]) is injected into the LHD edge. Figure 1 shows the typical time evolutions of ablation light of TESPEL, stored energy, line-averaged electron density n_e,and T_e at different radii. Typical parameters in this experiment are: neutral beam injection (NBI) power 2–4 MW, R_{ax} = 3.5–3.6 m, and B_{ax} = 2.75–2.95 T, with a minor radius of 0.6 m.

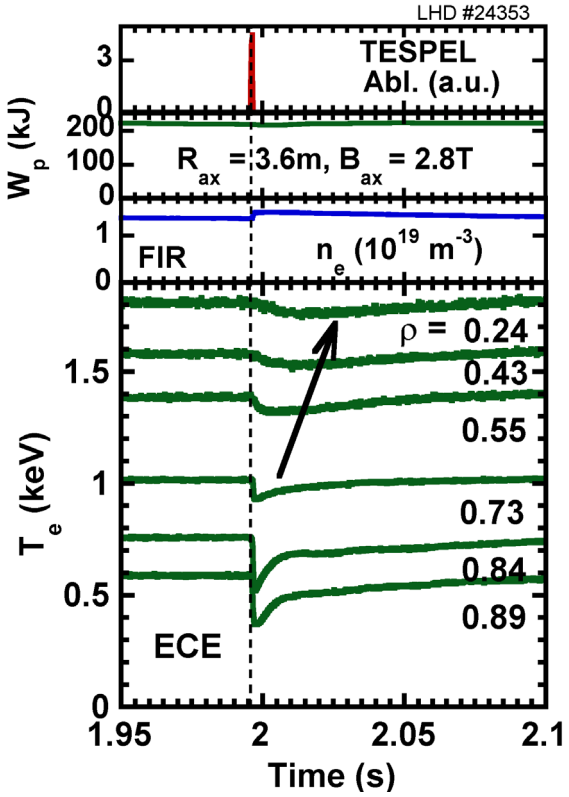

Fig. 1. Typical time evolutions of plasma perturbations induced by the TESPEL injection in LHD.

The increase in density is consistent with the contribution of the electrons brought to the plasma by the TESPEL. The total input power is kept constant and the change in the stored energy is less than 3% and thereby the global confinement is not affected by TESPEL injection. The TESPEL typically penetrates into the normalized radial region of $\rho \sim 0.6$. The transient transport analysis is carried out with a simple nonlinear model for χ_e, $\chi_e \propto T_e^{\alpha} |\nabla T_e|^{\beta}$. Using this model, the perturbed electron heat transport equation can be written as

$$\frac{3}{2} n_e \frac{\partial \delta T_e}{\partial t} = \nabla \cdot \left(n_e (1+\beta) \chi_e \nabla \delta T_e - n_e \alpha \chi_e \frac{\delta T_e}{L_T} \right) \qquad (1)$$

Here n_e, ∇T_e, T_e, and χ_e are static values obtained just before TESPEL injection at $t = t_0$. $\delta T_e = T_e(\rho, t = t_0) - T_e(\rho, t > t_0)$, and χ_e can be estimated by static analysis,

(i.e., power balance analysis). The value of n_e increases in the ablation region ($\rho > 0.6$) while it does not change in the core region within the accuracy of the Abel inversion. The particle diffusivity, which is estimated by gas-puff modulation experiments [11], is much smaller than χ_e, and thus particle transport effects on the cold pulse propagation can be neglected in LHD. When the heat flux perturbation $\delta q_e(\rho, t)$, and the perturbation scale length, $L_{\delta T}$ are defined as

$$\delta q_e = \frac{1}{r}\int \frac{3}{2} n_e \frac{\partial}{\partial t} \delta T_e r dr, \qquad (2)$$

then Eq. (1) can be written as

$$\frac{\delta q_e}{n_e \delta T_e} = \frac{\chi_{tr}}{L_{\delta T}} - V_{tr}, \quad \chi_{tr} = (1+\beta)\chi_e, \quad V_{tr} = \frac{\alpha \chi_e}{L_T} \qquad (3)$$

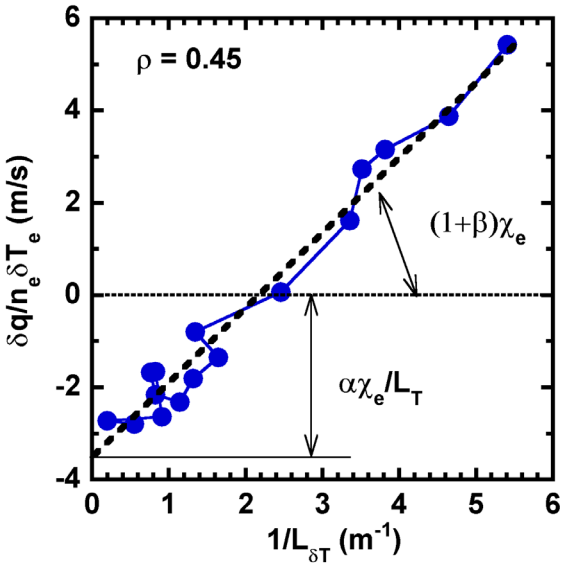

Fig. 2. Typical plasma behavior in the perturbed temperature gradient vs the perturbed heat flux space at $\rho = 0.45$.

Figure 2 shows a typical time trace of the plasma in gradient–flux space for cold pulse propagation. The fact that data points indeed lie on a straight line allows us to determine β and α from the slope and intercept of a line. The obtained χ_{tr} is shown in Fig. 3(a). The heat diffusivity estimated by power balance analysis, χ_{pb}, is also shown. The small difference between χ_{pb} and χ_{tr} indicates a weak ∇T_e dependence of χ_e ($\beta \sim 0$) in LHD. In contrast, a strong T_e dependence of χ_e is indicated in Fig. 3(b). A gyro-Bohm-like T_e dependence ($\alpha = 3/2$–$5/2$) can explain the obtained values for α. Although the value of α in the edge region is expected to have a strong influence on the global energy confinement, it has not been obtained by transient analysis. This T_e dependence of χ_e can be considered a candidate explanation for the power degradation of the global confinement in LHD.

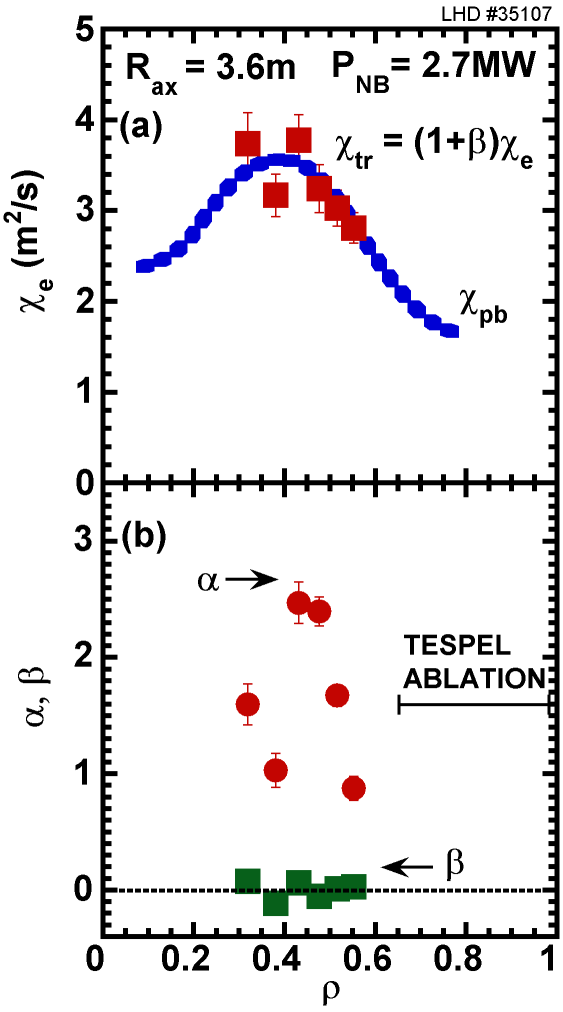

Fig. 3. Typical radial profiles of (a) χ_{tr} and χ_{pb}, and (b) α (the index of the T_e dependence of χ_e) and β (the index of the ∇T_e dependence of χ_e).

Cold pulse propagation in plasma with an electron internal transport barrier

The electron ITB (eITB) is formed when electron cyclotron heating (ECH) is focused on the magnetic axis in LHD (P_{ECH} ~0.8 MW, P_{NBI} ~2 MW, line-averaged density = 0.7×10^{19} m^{-3}). Neither ion nor n_e ITBs are present in LHD (T_{i0} = 1.8 keV). When the cold pulse propagation technique is used to perturb ITB plasmas, a unique feature of cold pulse propagation is observed. When the cold pulse approaches the ITB foot, the negative peak of the cold pulse is enhanced, as shown in Fig. 4(a). Here, no evidence of a significant plasma shift induced by the TESPEL injection is observed. The simple diffusive nature (heat

flux is proportional to temperature gradient) cannot explain this enhancement of the cold pulse.

Transient transport analysis shows a strong reduction of $\chi_{tr} = (1+\beta)\chi_e$ inside the ITB region [see Fig. 4(b)]. The small difference between χ_{tr} and χ_{pb} indicates that $\beta = 0$ (i.e., the ITB is in a "weak" or "not stiff" region). The growth of the cold pulse peak can be explained by the convective-like term driven by the T_e dependence of χ_e [see Eq. (1)] because the transient transport analysis indicates the negative T_e dependence of χ_e (χ_e decreases with an increase in T_e). Figure 4(c) shows the T_e dependence factor α and the ∇T_e dependence factor β of χ_e. The negative T_e dependence ($\alpha < 0$) is observed inside the ITB in LHD. The heat transport feature inside the ITB is different qualitatively from that outside the ITB in LHD. Although the physical mechanisms that could be responsible for this negative T_e dependence of χ_e are still unclear (no gyro-Bohm model can provide $\alpha < 0$), the negative T_e dependence may contribute to the ITB formation in LHD.

Summary

The perturbative technique is applied and the empirical nonlinear transport model is discussed in LHD. Cold pulses are induced with and without ITB plasmas in LHD. The experimental results show (1) no or weak ∇T_e dependence of χ_e in plasmas with and without an ITB, (2) the gyro-Bohm-like positive T_e dependence of χ_e in the no-ITB region, (3) reductions of χ_{tr} and χ_{pb} inside the ITB, and (4) enhancement of the cold pulse peak inside the ITB due to the negative T_e dependence of χ_e. These experimental results are very important to test some first-principle transport models.

S. Inagaki, K. Ida, N. Tamura, T. Shimozuma, S. Kubo, Y. Nagayama, K. Kawahata, S. Sudo, and LHD Experimental Group.

National Institute for Fusion Science
Oroshi-cho, Toki-shi
Gifu, 509-5292, Japan

E-mail: iinagaki@LHD.nifs.ac.jp

References

[1] W. Horton et al., Phys. Fluids **31** (1988) 2971.

[2] F. Romanelli and S. Briguglio, Phys. Fluids B **2** (1990) 754.

[3] F. Ryter et a.l, Phys. Rev. Lett. **86** (2001) 5498.

[4] H. Yamada et al., Nucl. Fusion **43** (2003) 749.

[5] J. Miyazawa et al., submitted to Plasma Phys. Control. Fusion.

[6] N. J. Lopes Cardozo, Plasma Phys. Control. Fusion **37** (1995) 799.

[7] T Shimozuma et al, Plasma Phys. Control. Fusion **45** (2003) 1183.

[8] A. Fujisawa et al., Phys. Rev. Lett. **82** (1999) 2669.

[9] U. Stroth et al., Phys. Rev. Lett. **86** (2001) 5910.

[10] S. Sudo et al., Plasma Phys. Control. Fusion **44** (2002) 129.

[11] K. Tanaka, "Experimental study of plasma transport and density fluctuations in LHD," presented at the 20th IAEA Fusion Energy Conference, Villamoura, Portugal, November 2004; to be submitted to Nucl. Fusion.

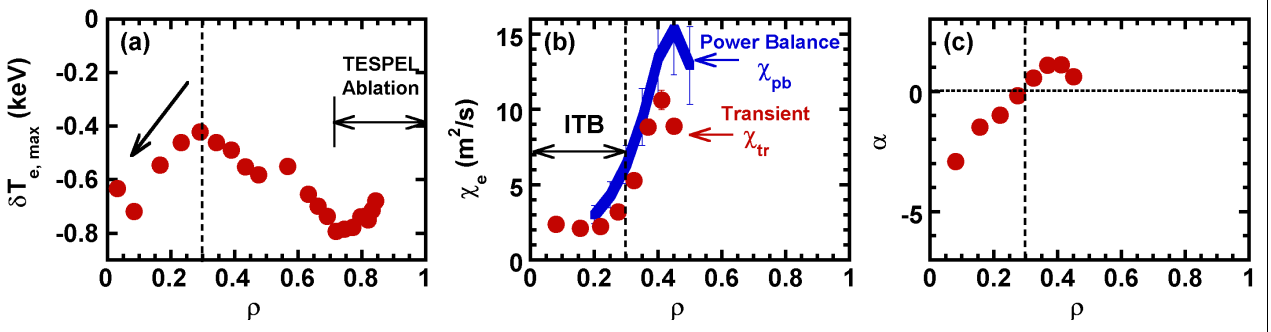

Fig. 4. Radial profiles of (a) the cold pulse peak, (b) χ_{tr} and χ_{pb}, and (c) the T_e dependence of χ_e in a plasma with eITB.

Electron Bernstein wave heating in the TJ-II stellarator

In contrast to electron cyclotron (EC) electromagnetic waves, electron Bernstein waves (EBWs) are quasi-electrostatic perturbations that can propagate in plasmas without any cut-off density limit. For TJ-II plasmas, the excitation of these waves is based either on the direct X-B mode conversion (from the high-field side), in which the slow X mode is transformed at the upper hybrid resonance (UHR) into a Bernstein mode, or on the O-X-B mode conversion (from the low-field side), in which the initial O mode is first converted into the slow X mode near the O mode cut-off surface, and finally transformed into a Bernstein mode when approaching the UHR layer.

EBWs have been successfully used to heat overdense plasmas in the W7-AS [1] and Heliotron-J [2] stellarators. Since there is no density limit, plasma heating with EBWs allows one to reach higher collisionality physics and to get a good plasma target for neutral beam injection (NBI) heating. EBWs can also be used to drive currents [2] and to perform perturbative experiments.

The Clemmov-Mullaly-Allis (CMA) diagram in the EC frequency range shows that the X-B2 heating scheme (X-B conversion at second harmonic) is not feasible in TJ-II [3] since the magnetic field variation inside the plasma does not exceed 30–35%, whereas it should be greater than 100%. Moreover, the O-X-B1 and O-X-B2 schemes are not practicable in plasmas with $n_{max} < n_{O\text{-}X}$ (where $n_{O\text{-}X}$ is the O-mode cut-off density). The central densities for O-X conversion in TJ-II ($B_0 < 1$ T) are $n_0 \approx 1.1 \times 10^{19}\,\mathrm{m}^{-3}$ for O-X-B1 ($f = 28$ GHz) and $n_0 \approx 3.8 \times 10^{19}\,\mathrm{m}^{-3}$ for O-X-B2 ($f = 53.2$ GHz). TJ-II plasmas are created by two gyrotrons (53.2 GHz, 300 kW, 1 s) coupling the power to the X polarization mode, and therefore the O-X-B2 conversion is also unfeasible since $n_{O\text{-}X} > n_{max} \equiv n_{cut\text{-}off} \approx 1.7 \times 10^{19}\,\mathrm{m}^{-3}$.

Thus, the only heating schemes that can be used in TJ-II are X-B1 and O-X-B1. The X-B1 may be problematic in high-density plasmas with $n_{max} > 1.9 \times 10^{19}\,\mathrm{m}^{-3}$ because the central region is opaque to X-mode, while peripheral propagation suffers from strong refraction. For this reason, and because of the restricted access to the launching position inside the TJ-II vacuum vessel, the O-X-B1 scenario has been chosen. When n_0 drops below $1.1 \times 10^{19}\,\mathrm{m}^{-3}$, O-X conversion fails. Therefore, second harmonic X mode ECH must be used to obtain a plasma with the appropriate density, and extra gas puffing must be performed to achieve the final density needed for good peripheral O-X conversion.

The ray tracing code TRUBA has been developed in order to study the properties of propagation, absorption, and mode conversion of EC waves in the specific three-dimensional (3-D) TJ-II geometry [4]. To determine the best launching position, a single ray with optimum parallel index of refraction $N_{||}$ for O-X conversion has been traced from different starting points [5]. The chosen position has the most centered (closest to the plasma center) and localized power deposition. The result of ray tracing calculations for this heating scheme is presented in Fig. 1. The optimum Gaussian beam, in terms of O-X conversion efficiency, was also determined [5].

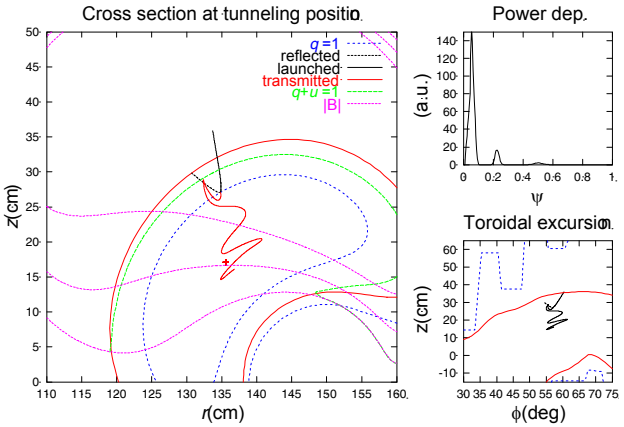

Fig. 1. Ray trajectory and power deposition profile for the optimum launching position [where $q \equiv (\omega_{pe}/\omega)^2$, $u \equiv (\omega_{ce}/\omega)^2$] of the O-X-B1 scenario.

A system to carry out these experiments has been designed [6]. The 28-GHz, 300-kW, 100-ms gyrotron was previously used for EC plasma heating in the TJ-IU stellarator. A new high-voltage power supply unit, which provides the formation of a stabilized negative voltage pulse up to 70 kV and a maximum current of 25 A, has been designed for this gyrotron. Assembly and installation will be completed during the second term of 2005.

The microwave power will be transmitted by a 45-mm oversized corrugated waveguide with two 90º continuous bends. Two ellipsoidal mirrors are necessary to optimize the Gaussian beam parameters at the input of the waveguide. Two corrugated mirrors are used to obtain the optimal polarization, so that the highest O-X conversion efficiency can be achieved. Finally, a movable internal mirror is needed in order to focus the beam and to overcome the restrictive launching angle conditions. In Fig. 2 the general scheme of the system is shown. Figure 3 shows a detail of the launching sector and the internal mirror.

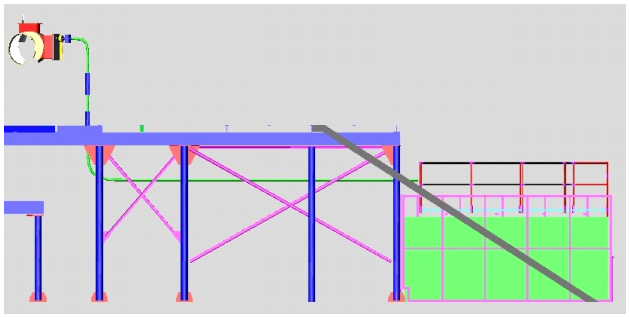

Fig. 2. Layout of the system. EBW launching sector, transmission line, and gyrotron area are represented.

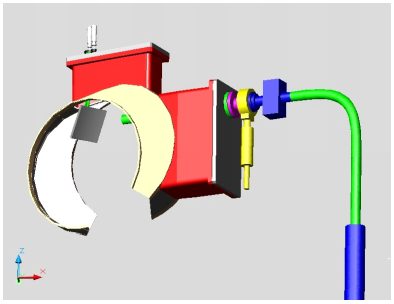

Fig. 3. Last bend of the corrugated transmission line and internal movable mirror.

The present cooling system of the EC system is being upgraded to cool the 28-GHz complex. The extension of the system will include the water supply for the gyrotron, the high-voltage power supply, and a calorimetric system to measure the gyrotron output power.

The start of the experiments is scheduled for the last term of 2005.

A. Fernández,[1] F. Castejón,[1] A. Cappa,[1] K. Sarksyan,[2] N. Matveev,[3] M.Tereshchenko,[2] J. Doane,[4] A. García,[1] M. Medrano,[1] J. Doncel,[1] A. Pardo,[1] N. Khartchev,[2] A. Tolkachev[1]

[1]EURATOM-CIEMAT Association for Fusion, Avda. Complutense 22, 28040 Madrid, Spain
[2]General Physics Institute, Russian Academy of Sciences, Moscow, Russia
[3]State Unitary Enterprise "All-Russian Electrotechnical Institute," Moscow, Russia
[4]General Atomics, San Diego, California, USA

E-mail: angela.curto@ciemat.es

References

[1] H. Laqua et al., Nucl. Fusion **43** (2003), 1324.

[2] K. Nagasaki et al., "Electron Bernstein wave heating in Heliotron Systems," Proc. EC12. Aix en Provence, France (2002).

[3] F. Castejón et al., Fusion Sci. and Technol. **46** (2004) 327.

[4] M.Tereshchenko et al. "Development and use of 3D Ray/Beam Tracing code for plasma heating by EBW in the TJ-II stellarator." Proc. of the 30th EPS, Europhysics Conference Abstracts 27 A.

[5] A.Cappa et al., "EBW launching optimization in TJ-II." Proc. 31st EPS Conference on Controlled Fusion and Plasma Physics, London, 2004, Europhy. Confe. Abstr. 28B, paper P4-175.

[6] A.Fernández et al., Fusion Science and Technology. **46** (2004) 335.